often formulated in the context of classical mechanics. To elucidate further the mechanisms of proton motion, future investigations of this system will be undertaken on deuterated analogs.

That the moiety that displays coherent proton tunneling is not the ground state of the system is of interest and worthy of further examination. The energy characterizing the growth of the tunneling peak, $D = (125 \pm 10)k_B$ K, is relatively small and of similar magnitude to the energy differences between tautomers related, for example, by proton transfer in carboxylic acid dimers and in the closely related molecule tBC (*10*). Examination of the spectral density recorded on calix[4]arene as in Fig. 2A reveals the presence of two identifiable incoherent components related to thermally activated stochastic proton-hopping processes. One of these, which we shall label process 1, has characteristics analogous to the proton transfer process reported in earlier observations in tBC and is modeled well by incoherent proton tunneling in a DWP with asymmetry D. Therefore, we propose that process 1 is the mechanism by which the moiety that exhibits coherent tunneling becomes populated. One way this can be realized is if the potential energy surface related to proton transfer in a particular molecule is influenced by the tautomeric state of its neighboring molecules. As neighboring molecules undergo incoherent tunneling with fast exchange on the time scale of ω_t, and as the temperature becomes sufficiently high to substantially populate both wells of the neighbor's asymmetric DWP, so the asymmetry for the moiety in question may become close to zero and permit the coherent tunneling processes we observe to mediate proton transfer. Precedence for this model is provided by the distortion of the crystal field that arises from the introduction of optical probe molecules in benzoic acid (*14*), although in that case, the distortions are static.

The second incoherent thermally activated proton-hopping process observed, which we shall label process 2, is much slower, with classical Arrhenius behavior described by correlation time $\tau_c = 1.2 \times 10^{-12} \exp(900/T)$s. The activation energy is $\Delta E_{act}/k_B = 900$ K, and it is proposed that this process may be assigned to rotational flips of the O-H groups, giving rise to H bond flip-flop motion of the kind advocated by Saenger *et al.* (*15*) and observed by Bernhard *et al.* in Dianin's compound (*16*). Additional experiments will be required to investigate this process, but in our data, it appears to be independent and separate from the coherent tunneling motion.

The observation of discrete tunneling frequencies associated with translational atomic displacements is rare. Tunneling associated with proton transfer in H bonds has been observed by microwave spectroscopy in the gas phase where the molecules are well isolated (*17*). In the solid state, coherent tunneling associated with proton transfer has been uniquely observed in doped benzoic acid where optical probes in low concentration introduce a crystal field distortion for a shell of molecules in the immediate vicinity that is just sufficient to offset the energy asymmetry characteristic of the bulk material; the tunneling frequency is 8.4 GHz (*14*). In this report, we have described coherent proton tunneling with a frequency of 35 MHz in a hydrogen bond network; also important is the coupling between hydrogen bonds that the spectra reveal. These findings will be important both to our understanding of processes relevant to the life sciences and to the fundamental role played by tunneling in chemical dynamics.

References and Notes

1. A. Kohen, R. Cannio, S. Bartolucci, J. P. Klinman, *Nature* **399**, 496 (1999).
2. N. S. Scrutton, J. Basran, M. J. Sutcliffe, *Eur. J. Biochem.* **264**, 666 (1999).
3. D. Diamond, M. A. McKervey, *Chem. Soc. Rev.* **25**, 15 (1996).
4. N. Bloembergen, E. M. Purcell, R. V. Pound, *Phys. Rev.* **73**, 679 (1948).
5. R. Kubo, K. Tomita, *J. Phys. Soc. Jpn.* **9**, 888 (1954).
6. D. F. Brougham, A. J. Horsewill, R. I. Jenkinson, *Chem. Phys. Lett.* **272**, 69 (1997).
7. C. P. Cheng, T. L. Brown, *J. Am. Chem. Soc.* **101**, 2327 (1979).
8. M. Torkar, V. Zagar, J. Seliger, *J. Magn. Reson.* **144**, 13 (2000).
9. A. J. Horsewill, *Prog. Nuclear Magn. Reson. Spectrosc.* **35**, 359 (1999).
10. D. F. Brougham, R. Caciuffo, A. J. Horsewill, *Nature* **397**, 241 (1999).
11. J. Haupt, *Z. Naturforsch.* **26a**, 1578 (1971).
12. F. Aguilar-Parrilla *et al.*, *J. Am. Chem. Soc.* **114**, 9657 (1992).
13. J. L. G. de Paz *et al.*, *J. Chem. Soc. Perkin Trans.* **2**, 101 (1997).
14. A. Oppenländer, Ch. Rambaud, H. P. Trommsdorff, J. C. Vial, *Phys. Rev. Lett.* **63**, 1432 (1989).
15. W. Saenger, Ch. Betzel, B. Hingerty, G. M. Brown, *Nature* **296**, 581 (1982).
16. T. Bernhard, H. Zimmerman, U. Haeberlen, *J. Chem. Phys.* **92**, 2178 (1990).
17. S. L. Baughcum, R. W. Duerst, W. F. Rowe, Z. Smith, E. B. Wilson, *J. Am. Chem. Soc.* **103**, 6296 (1981).

18. N.H.J. is sponsored by an Engineering and Physical Sciences Research Council postgraduate research scholarship. We are grateful to F. Ugozzoli for preparing the sample and for discussions with M. E. Smith.

8 September 2000; accepted 20 November 2000

Photoactivated Fluorescence from Individual Silver Nanoclusters

Lynn A. Peyser, Amy E. Vinson, Andrew P. Bartko, Robert M. Dickson*

Fluorescence microscopy of nanoscale silver oxide (Ag_2O) reveals strong photoactivated emission for excitation wavelengths shorter than 520 nanometers. Although blinking and characteristic emission patterns demonstrate single-nanoparticle observation, large-scale dynamic color changes were also observed, even from the same nanoparticle. Identical behavior was observed in oxidized thin silver films that enable Ag_2O particles to grow at high density from silver islands. Data were readily written to these films with blue excitation; stored data could be nondestructively read with the strong red fluorescence resulting from green (wavelengths longer than 520 nanometers) excitation. The individual luminescent species are thought to be silver nanoclusters that are photochemically generated from the oxide.

The strength of nanoparticle absorption and emission enables facile observation of single particles (*1, 2*) with much higher and often more robust signals than those produced by organic dyes (*3–5*). Such single-particle observations have furthered understandings of heterogeneity in molecular behavior (*6–8*). Complementary to environment-influenced single-molecule dynamics (*5, 7*), nanoparticles are larger, more complex systems, and their fluorescence often reflects the nanoparticle/surface interactions that affect electron-hole recombination (*1, 2*). However, the utility of nanoparticles would be greatly enhanced if their fluorescence were designed to be "caged" or photoactivated. Such caged fluorescent particles could be rapidly switched on and used, for example, as nanoscopic optical storage elements or as probes in living systems. Although photochromic molecules have been observed as single fluorescent entities (*6*), to date no photoactivated fluorescent nanoparticles have been produced to the best of our knowledge, let alone ones that are observable on a single-particle level. Such caged fluorescence should prove easier to observe from small clusters that are photochemically generated from, yet stabilized by, a surrounding solid

---

School of Chemistry and Biochemistry, Georgia Institute of Technology, Atlanta, GA 30332–0400, USA.

*To whom correspondence should be addressed. E-mail: dickson@chemistry.gatech.edu

matrix. Although many photochemical transformations are known, none yet produce strongly fluorescent photoproducts from initially nonfluorescent nanoparticles.

In photography, photoreactions produce small, surface-bound Ag clusters from silver halide particles, the fluorescence of which has recently been reported (*9*). Although not yet harnessed for applications, strong visible fluorescence has also been demonstrated from both neutral and charged small Ag clusters (two to eight atoms) in rare gas matrices (*10–15*). Even silver oxide (Ag_2O), which readily produces large surface-enhanced Raman signals resulting from photoinduced Ag cluster formation (*16–19*), has, to our knowledge, not been studied with fluorescence microscopy. Because it has a band gap in the visible region (2.25 eV or ~550 nm) (*20*) and is readily photoreduced to yield metallic Ag clusters (*16*), Ag_2O provides a possible route to producing potentially fluorescent moieties upon visible illumination.

In order to study nanoscale materials with photoactivated fluorescence, solid Ag_2O [99.9% (Aldrich Chemical, Milwaukee, Wisconsin), or formed by combining $AgNO_3$ with KOH in aqueous solution] was ground, suspended in $CHCl_3$, and sonicated to break up larger aggregates. After settling, the supernatant was placed on a cover slip, and the chloroform was allowed to evaporate. Nanoscale (~80-nm diameter) particles were created in this manner, as determined by dynamic light scattering and atomic force microscopy (AFM). Higher densities of much smaller Ag_2O particles (10 to 30 nm as determined from AFM and electron microscopy) were produced by the rapid oxidation of very thin Ag films. The Ag films were prepared in darkness by thermally evaporating Ag onto glass at a deposition rate of 1 Å/s with final thicknesses of 10.2, 11.5, 16.6, 18.2, 19.8, 30.4, 35.0, and 42.5 nm. On the thin films (<20 nm) used here, the presence of Ag_2O upon exposure to air was confirmed by x-ray photoelectron spectroscopy (XPS); only unoxidized metallic Ag was observed on thicker films. On these films, no Ag_2S was observed over the lifetime of the samples. Although oxide growth on homogeneous Ag films is self-passivating, Ag films thinner than ~20 nm are not homogeneous but form islands to minimize overall surface energy (*21*); thicker films (>30 nm), however, produce much more homogeneous coverage. Thus, Ag island formation is crucial to creating Ag_2O films because Ag_2O quickly overtakes Ag through the reactive, air-exposed, higher energy crystal faces. Both types of Ag_2O samples exhibited similar behavior, but the higher density films with smaller features are emphasized here. Samples were optically excited and observed from both sides of the Ag film (*8*) to ensure that exciting or collecting emission through different thicknesses of Ag did not affect the results.

Fluorescence from these dry, light-shielded Ag_2O samples was studied under both bandpass-filtered mercury lamp and Ar^+ laser (514.5 and 488.0 nm) excitation (*8*). In these samples, we observed that Ag_2O is initially nonfluorescent; however, upon illumination with wavelengths shorter than ~520 nm, multicolored fluorescence slowly grows in, one nanoparticle at a time. Once photoactivated, Ag_2O films exhibit bright multicolored fluorescence under both blue (450 to 480 nm) and green (510 to 550 nm) excitation. Although the average Ag_2O particle size is substantially greater than the nanometer scale, emission appeared from many localized sites, each of which exhibited distinctive emission patterns characteristic of single Ag nanoclusters (Fig. 1) (*8*). Once uncaged, very strong multicolored intermittent fluorescence, or "blinking," was clearly observed under continuous blue excitation. Under green excitation, however, even brighter and substantially more stable (that is, less intermittent) red fluorescence was observed. Typical blinking traces and on-time histograms under blue and green excitation (Fig. 2) not only further demonstrate single-particle behavior (*1, 4, 6, 22*), but also demonstrate a spectral dependence of the blinking dynamics. The clear asymmetries of single-particle emission patterns coupled with observed blinking dynamics nondestructively confirm single-particle behavior. This photoactivated emission represents a newly identified type of nanoparticle behavior that is readily observable on a single-particle level, even with weak mercury lamp excitation.

The necessity of Ag_2O formation for caged fluorescence is confirmed by the observation that thick (>30 nm) Ag films showed no emission, even after strong illumination with blue light, whereas thin films were highly fluorescent after photoactivation. Only films that are too thin to support a homogeneous Ag layer exhibit fluorescence, so island formation must occur such that oxide growth is not self-passivating. Thus, the emissive moiety is photochemically generated from the surrounding semiconductor to produce a Ag/Ag_2O chromophore with an extremely high absorption cross section, σ. Through saturation intensity measurements ($I_{sat} \sim 200$ W/cm^2 at 514.5 nm) and comparison to known single molecules [1,1′-dioctadecyl-3,3′,3-3′-tetramethylindocarbocyanine perchlorate, or $DiIC_{18}(3)$; $I_{sat} \sim 10{,}000$ W/cm^2] (*3*), the absorption cross section of our nanoparticles has been determined to be $\sigma \sim 8 \times 10^{-15}$ cm^2, a factor of 50 stronger than the best organic molecules [e.g., $DiIC_{18}(3)$, where $\sigma \sim 1.6 \times 10^{-16}$ cm^2] (*3*). In all cases, the highest density of emissive sites was observed on obviously oxidized samples.

The spectral dynamics of these individual features are even more surprising than is the observed wavelength dependence of the fluorescence intermittency. Although spectral diffusion has been observed in many single-nanoparticle or single-molecule systems (*2, 5*), our individual emissive particles produced dynamic single-particle color changes among red, green, and yellow in a seemingly random fashion. Such large shifts in emission wavelength (>100 nm) were previously unknown, but they were observed in these samples when photoactivated by and further excited with blue (but not green) light. Photographs of individual features clearly reveal such fluorescence spectral dynamics, with green, red, and yellow all being observed over time from the same nanoparticle (Fig. 1B). The additional observation of multicolored single-particle emission patterns (*8*) shows that individual particles can drastically change emission frequencies (Fig. 1C) and that this change

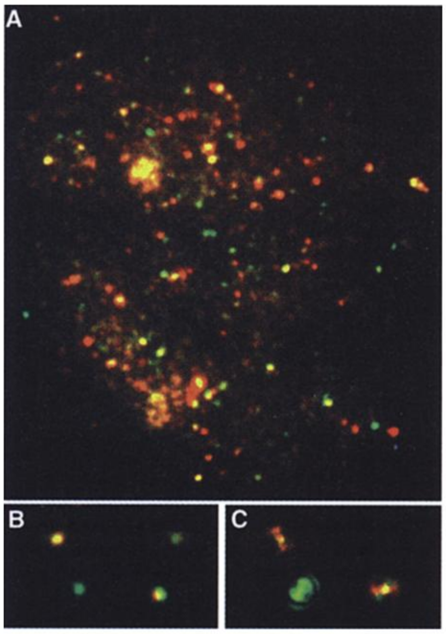

Fig. 1. (**A**) Fluorescence from a 16.6-nm Ag/Ag_2O film excited at 514.5 nm. (**B**) Four individual features and (**C**) each of these particles' emission patterns, confirming single-nanoparticle emission. The fluorescent nanoparticle in the upper right corner of (B) bleached between photographs. These individual nanoparticles emit as single-quantum systems that vary widely in emission wavelength under Ar^+ laser excitation. Similar behavior was observed under 488-nm Ar^+ laser and blue (450 to 480 nm) mercury lamp excitation. Excitation was performed at ~35.8 W/cm^2 in a standard epifluorescence geometry on an Olympus IX-70 inverted microscope using a 1.4 numerical aperture Plan-Apochromat objective (color corrected at three wavelengths). These photographs were taken with ISO 400 film with ~10-s exposures. The image in (A) is 29.5-μm wide. In (B), the upper two molecules are separated by 4.0 μm; (C) is on the same scale as (B).

cannot result from several particles emitting from the same diffraction-limited volume.

Although Ag_2O must absorb the incident radiation, the photoactivation indicates that photochemical change produces Ag atoms and silver peroxide [AgO, best described as a combination of Ag(I) and Ag(III)] (*16*), the latter of which is unstable at room temperature relative to Ag_2O (*23*) and readily photoreduced to form Ag^0 and 1/2 O_2 (*24*). Thus, we also prepared AgO samples similar to those for Ag_2O. Such samples of AgO (Aldrich Chemical) initially exhibited only very weak yellow fluorescence, but they were also quickly photoactivated to yield the diverse colors observed from both Ag_2O and oxidized Ag films. Because Ag_2O photochemically produces AgO (*16*) and because both oxides not only yielded Ag clusters upon irradiation but also produced photoactivated multicolored fluorescence, the more stable Ag_2O must be the caged species yielding the observed fluorescence. Once a metallic impurity is formed, it becomes easier to continue the photoreduction process, creating Ag_2^+, Ag_2, Ag_3^+. . ., but this is balanced by the relative instability of AgO and the binding energy of each cluster relative to the excitation energy (*10, 14*). This photochemical process enables small Ag clusters to form from Ag_2O crystals (and subsequently from AgO) similar to those harnessed in silver halide–based photographic emulsions. Such small Ag clusters are known to produce strong visible fluorescence (*10–15*) and should exhibit emission wavelength changes as they change geometry (*25, 26*) and size in the range from two to four atoms (*9, 11, 14*). Because the Ag cluster size and charge are constantly being modified under illumination and chemical reaction, it is not surprising that the emission color of individual emissive sites changes.

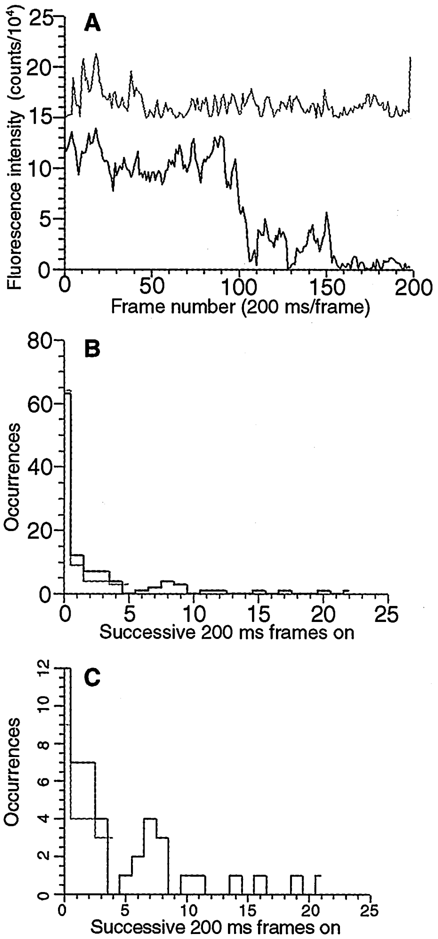

Fig. 2. (**A**) Typical single-particle blinking traces for blue-excited (450 to 480 nm, offset by 150,000 counts, gray line) and green-excited (510 to 550 nm, black line) fluorescence acquired for 200 frames with 200-ms time resolution, each at an intensity of ~30 W/cm^2. Thresholding 93 such traces at 2.5 times the data set's average intensity for each blue- and green-excited fluorescence trajectory yielded the on-time histograms plotted in (**B**) and (**C**). "On times" less than two frames long were discarded in (B); on times less than three frames were discarded in (C) to emphasize the difference in long on-time behavior between green- and blue-excited emission. The green-excited (i.e., red) fluorescence was much more stable, lasting for much longer periods of time.

The wavelength-dependent photoactivation, blinking, and spectral diffusion of blue-excited fluorescence, both on oxidized films and on Ag_2O nanocrystals, clearly indicate that the Ag_2O must absorb and form small neutral and cationic clusters of Ag metal and AgO, with subsequent energy transfer to and fluorescence from the Ag clusters. Thus, whereas the Ag clusters fluoresce under both blue and green illumination, the strong intermittency and dynamic color changes indicate that the surrounding Ag_2O likely absorbs the incident blue radiation and transfers energy to the Ag clusters. However, because the blinking and spectral diffusion under green excitation are greatly reduced, the Ag clusters are likely directly excited by longer wavelengths. This wavelength dependence matches extremely well with the known band gap for Ag_2O (*20*) and with the known green absorption and red emission lines of Ag clusters (*10–15*). The enhanced stability of the photoactivated red fluorescence excited by green light enables data to be written with blue light and nondestructively read with green, even on a single-particle level. Although the Ag_2O particles are 10 to 30 nm in size, the emissive site must consist of small Ag clusters, either within or on the surface of the Ag_2O crystals. Thus, the Ag_2O serves as the photoactivable material and may simultaneously provide a protective overcoating that stabilizes the uncaged Ag-cluster fluorescence.

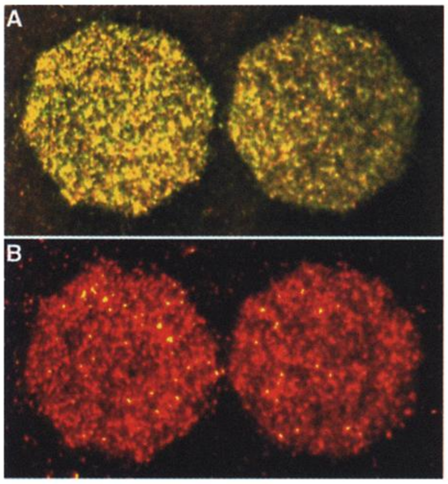

Fig. 3. (**A**) A photograph of two adjacent images of an aperture successively written to a Ag_2O film with blue mercury lamp excitation. (**B**) Red fluorescence from the same region as in (A) but illuminated with green light to nondestructively probe the images written with blue light. Photographs were taken with ISO 400 film with ~10-s exposures. Opposite vertices of each aperture are 35 μm apart.

Because each individual particle is photoactivated, data are readily stored in and nondestructively read from these high-density nanoparticle films. Blue mercury lamp illumination enabled images of a field aperture to be written on the Ag_2O films. Two adjacent images were successively written on the same film, each with a 10-min exposure at an intensity of ~30 W/cm^2 (Fig. 3). Although some emissive centers do seem to emit yellow light, images primarily grow in as individual red and green emissive sites. The final high-density images, however, exhibit only bits of red and green colors, which indicates that the yellow images result from color mixing of the dynamic red and green emission observed under blue excitation. Because blue light continues to write information, reading data with blue excitation will degrade data integrity. Because these emissive features also absorb green light with concomitant stable red emission, these same features can be nondestructively read by green illumination, even up to many hours after being written, without substantial image degradation. Reading data with green excitation very slowly bleaches the written image without substantially increasing the background. Blue excitation, however, maintains nearly constant intensity in the written image because of the equilibrium resulting from photoactivation and bleaching, but the background intensity markedly increases. This newly identified class of nanoparticle behavior offers the potential to photochemically control fluorescent spectral features on both the single-nanoparticle and bulk levels.

References and Notes

1. M. Nirmal, L. Brus, *Acc. Chem. Res.* **32**, 407 (1999).
2. S. Empedocles, M. Bawendi, *Acc. Chem. Res.* **32**, 389 (1999).

3. J. J. Macklin, J. K. Trautman, T. D. Harris, L. E. Brus, *Science* **272**, 255 (1996).
4. D. A. Vanden Bout *et al.*, *Science* **277**, 1074 (1997).
5. W. E. Moerner, M. Orrit, *Science* **283**, 1670 (1999).
6. R. M. Dickson, A. B. Cubitt, R. Y. Tsien, W. E. Moerner, *Nature* **388**, 355 (1997).
7. X. S. Xie, *Acc. Chem. Res.* **29**, 598 (1996).
8. A. P. Bartko, R. M. Dickson, *J. Phys. Chem. B* **103**, 11237 (1999).
9. A. P. Marchetti, A. A. Muenter, R. C. Baetzold, R. T. McCleary, *J. Phys. Chem. B* **102**, 5287 (1998).
10. L. König, I. Rabin, W. Schulze, G. Ertl, *Science* **274**, 1353 (1996).
11. W. Harbich *et al.*, *J. Chem. Phys.* **93**, 8535 (1990).
12. S. Fedrigo, W. Harbich, J. Buttet, *J. Chem. Phys.* **99**, 5712 (1993).
13. C. Felix *et al.*, *Chem. Phys. Lett.* **313**, 105 (1999).
14. I. Rabin, W. Schulze, G. Ertl, *J. Chem. Phys.* **108**, 5137 (1998).
15. T. Tani, M. Murofushi, *J. Imaging Sci. Technol.* **98**, 1 (1994).
16. R. Kotz, E. Yeager, *J. Electroanal. Chem.* **111**, 105 (1980).
17. E. S. Brandt, *Appl. Spectrosc.* **47**, 85 (1993).
18. X. Q. Wang *et al.*, *Spectrochim. Acta A* **53**, 2495 (1997).
19. T. Watanabe, O. Kawanami, K. Honda, B. Pettinger, *Chem. Phys. Lett.* **102**, 565 (1983).
20. A. J. Varkey, A. F. Fort, *Sol. Energy Mater. Sol. Cells* **29**, 253 (1993).
21. T. Yamaguchi, S. Yoshida, A. Kinbara, *J. Opt. Soc. Am.* **64**, 1563 (1974).
22. H. P. Lu, L. Y. Xun, X. S. Xie, *Science* **282**, 1877 (1998).
23. H. Libardi, H. P. Grieneisen, *Thin Solid Films* **333**, 82 (1998).
24. B. Ohtani, S.-W. Zhang, T. Ogita, S. Nishimoto, T. Kagiya, *J. Photochem. Photobiol. A* **71**, 195 (1993).
25. P. S. Bechthold, U. Kettler, H. R. Schober, W. Krasser, *Z. Phys. D* **3**, 263 (1986).
26. I. Rabin *et al.*, *Chem. Phys. Lett.* **320**, 59 (2000).
27. We acknowledge stimulating discussions with R. L. Whetten and experimental assistance from L. A. Lyon and Z. L. Wang, and we gratefully acknowledge partial support of this project by the Georgia Institute of Technology Molecular Design Institute, under prime contract N00014-95-1-1116 from the Office of Naval Research and by the NSF Research Experiences for Undergraduates Program.

29 August 2000; accepted 20 November 2000

Toward Separation and Purification of Olefins Using Dithiolene Complexes: An Electrochemical Approach

Kun Wang* and Edward I. Stiefel*

The complex $Ni[S_2C_2(CF_3)_2]_2$ reacts with light olefins, including ethylene and propylene, selectively and reversibly. The reaction is not poisoned by hydrogen gas, carbon monoxide, acetylene, or hydrogen sulfide, which are commonly present in olefin streams, presumably because olefin binding occurs through the sulfur ligand rather than the metal center. The reversible reaction of olefins with $Ni[S_2C_2(CN)_2]_2^n$ ($n = 0, -1, -2$) can be controlled electrochemically, where the oxidation state–dependent binding and release of olefins are fast on the electrochemical time scale. The observed tolerance to poisons and controllable electrochemical reactivity present an alternative approach to the separation of olefins from complex streams.

Olefins are the largest volume feedstock in the chemical and petrochemical industry, and are widely used in the production of polymers, acids, alcohols, esters, and ethers (*1*). The lightest olefin, ethylene, is the largest volume organic chemical (*2*). Generally, olefins are produced via steam or catalytic cracking (*3, 4*) and separated by cryogenic distillation. The latter process is energy-intensive and costly, and contributes ~75% of the total olefin production cost (*5*). The large volume of olefins produced and the required purity for most applications provide strong incentives for novel alternative separation approaches.

The use of chemically specific separation reagents driven by electrical energy is a potentially inexpensive and efficient approach for separation (*6*). Indeed, redox-active metal salts such as copper (*7, 8*) have been reported to react with olefins reversibly. However, these metal-based systems are poisoned by C_2H_2, CO, and H_2S. Sulfur-containing systems such as those reported by DuBois *et al.* (*9*) might be tolerant to H_2S and CO, but react with H_2 and C_2H_2.

We report a reversible and robust system for olefin separation based on metal 1,2-ene-dithiolate (dithiolene) complexes. Whereas early interest in dithiolene complexes focused on their unusual redox and optical properties (*10–13*), recent studies have ranged from bioinorganic chemistry to material science (*14–16*). Schrauzer *et al.* (*17*) reported that $M(S_2C_2Ph_2)_2$ (M = Ni, Pd, Pt; Ph = phenyl group) reacts with norbornadiene, and Wing *et al.* (*18, 19*) reported that $Ni[S_2C_2(CF_3)_2]_2$ (**1**) reacts with norbornadiene and 2,3-dimethyl-1,3-butadiene to form 1/1 olefin adducts, where the olefin binds to ligand S atoms rather than the metal. However, there are no reports of such reactions with light unstrained mono-olefins. We found that, under mild conditions, **1** reacts with simple, aliphatic olefins selectively and reversibly to form 1/1 adducts.

Upon reaction with olefins, the deep purple solution of **1** turns light yellow, and the intensity of the lowest energy band (744 nm) in the ultraviolet-visible (UV-vis) spectrum decreases. The band at 744 nm [molar extinction coefficient $\varepsilon = 1050$ (toluene)] has been assigned as the transition between the highest occupied molecular orbital and the lowest unoccupied molecular orbital (HOMO→LUMO transition). When the adduct can be isolated (such as for norbornene and norbornadiene), the 744-nm band is absent. With simple olefins, the bands at 744 and 570 nm decrease with time (but do not fully disappear), and a band at 420 nm simultaneously appears, with an isosbestic point at 442 nm (Fig. 1). Similar patterns are observed for ethylene, propylene, *cis*-2-butene, 1-hexene, and *trans*-3-hexene. Exposure to an Ar atmosphere completely restores **1**, indicating that the reactions are fully reversible.

Low concentrations of H_2, CO, C_2H_2, H_2O, and H_2S may be present in typical olefin streams (*1*). These components generally poison metal-based complexing agents. However, when a solution of **1** (1 mM) was treated individually with pure (1 atm = 101.3 kPa) H_2, CO, C_2H_2, or water-saturated toluene under conditions used for ethylene binding, no reaction was observed. Moreover, the reaction with ethylene is not affected when 8 mole percent (~10 weight percent) H_2S is present, which is a far higher concentration than that found in typical olefin streams (*20, 21*). Clearly, **1** is tolerant to poisons potentially present in olefin streams, which we attribute to olefin binding at sulfur rather than the metal (Scheme 1). This unusual mode of olefin binding has been unambiguously demonstrated by x-ray crystallography for the norbornadiene adduct (*18*).

Kinetic studies were carried out using UV-vis spectroscopy for the reactions of 1-hexene and *trans*-3-hexene with **1**. Under pseudo–first order conditions, the plot of $\ln(A - A_e)$ versus time gives a straight line over three half-lives, revealing the reaction to be first-order in **1**. Plotting the observed rate constant k_{obs} against olefin concentration gives a straight line, indicating that the reaction is also first-order in olefin (Fig. 2). Consistent with a bimolecular reaction (Scheme 1) implied by the second-order kinetics, the mass spectrum (field desorption) of a solution of **1** in neat 1-hexene clearly shows a 1/1 adduct.

For ethylene and propylene, comparative

Corporate Strategic Research, ExxonMobil Research and Engineering Company, Route 22 East, Clinton Township, Annandale, NJ 08801, USA.

*E-mail: kwang@erenj.com (K.W.); eistief@erenj.com (E.I.S.)